Investigation of resonant and transient phenomena in Josephson junction flux qubits

Jeffrey E. Marchese,[1] Matteo Cirillo,[2] and Niels Grønbech-Jensen[1]
[1]*Department of Applied Science, University of California–Davis, Davis, California 95616, USA*
[2]*Dipartimento di Fisica and MINAS-Lab, Università di Roma "Tor Vergata," I-00173 Roma, Italy*
(Received 13 October 2008; revised manuscript received 1 January 2009; published 18 March 2009)

We present an analytical and computational study of resonances and transient responses in a classical Josephson junction system. A theoretical basis for resonances in a superconducting loop with three junctions is presented, outlining both the direct relationship between the dynamics of single- and multijunction systems and the direct relationships between observations of the classical counterparts to Rabi oscillations, Ramsey fringes, and spin-echo oscillations in this class of systems. We show simulation data along with analytical analyses of the classical model, and the results are related to previously reported experiments conducted on three junction loops. We further investigate the effect of off-resonant microwave perturbations to, e.g., the Rabi-type response of the Josephson system, and we relate this response back to the nonlinear and multivalued resonance behavior previously reported for a single Josephson junction. The close relationships between single and multijunction behaviors demonstrate the underlying dynamical mechanism for a whole class of classical counterparts to expected quantum-mechanical observations in a variety of systems, namely, the resonant and transient behavior of a particle in an anharmonic potential well with subsequent escape.

DOI: 10.1103/PhysRevB.79.094517 PACS number(s): 74.50.+r, 85.25.−j, 85.35.Ds

I. INTRODUCTION

Since the mid 1980s several experiments have sought to establish that Josephson systems show evidence of quantum interference of macroscopically distinct states. Various configurations have been utilized to elicit the phenomenon, including current-biased single-junction circuits,[1–5] flux-biased two-junction superconducting quantum interference devices (SQUIDs),[6] charge-biased two-junction SQUIDs,[7] flux-biased three-junction SQUIDs,[8–13] charge-biased three-junction SQUIDs,[14] and hybrid systems which often include inductor-based systems to create multiple potential wells.[15–19] The phenomena observed to date include multipeaked probability distributions in bias current, Rabi oscillations,[20] Ramsey fringes,[21] spin-echo oscillations,[22] and quantum tomography.[23]

In several recent investigations the authors of the present paper have contributed to an alternative interpretation of the basic types of experiments on Josephson junctions. This interpretation relies on the well-established phenomenology of the resistively and capacitively shunted junction (RCSJ) model[24] and on nonlinear dynamics related to it. Multipeaked resonances were addressed in Refs. 25–27, while Refs. 28 and 29 developed analytical expressions and presented computer simulations which described the relationships among classical Rabi-type oscillations, driving amplitude and frequency, and systematic dissipation. The related phenomena of Ramsey fringes and spin-echo oscillations are depicted and described from a classical point of view in Refs. 30 and 31. While this exemplifies the phenomena through current-biased single-junction circuits, we submit that a wide class of Josephson systems exhibits same behavior when a system variable is trapped in a potential well.[32] This presentation will amplify this point.

A few examples of multijunction systems for which direct comparisons between classical theory and experimental results have been made in the low-temperature regime, where quantum phenomena should be observed, include multipeaked resonances in Josephson interferometers, made of two junctions connected in parallel,[33] and a more complex Josephson interferometer-based device[34] containing a double SQUID in which a butterfly catastrophe was observed at 10 mK. In both cases, the standard classical RCSJ model provided sufficient detail to understand the experimental observations.

The observations from interferometer systems described in the last paragraph encouraged us[32] to extend the classical ideas and implementations developed for the single junction and two-junction interferometers to the more complex system of the flux-biased three-junction loop.[10–12,35] It is the plan of the present paper to report on our approach to this problem. In this approach the analysis of the most important features of three-junction loops under the influence of pulsed microwaves was preluded by a study of analogous single-junction phenomenology.

In Sec. II we derive the basic equations for the three-junction loop and present an analytical description of resonances in the system. In Sec. III we demonstrate computer simulations which map the resonances as a function of the biases (the magnetic flux in the loop). Simulations are shown which depict the Rabi-type oscillations, Ramsey-type fringes, and spin-echo-type oscillations in the three-junction loop. Also, off-resonant behavior in the three-junction loop is explored.

Our simulations and analytical treatment allow us to interpret the essential experimental features reported for Josephson circuits; the analysis shall all be based on the RCSJ modeling of Josephon circuits[24] that took origin from early remarks on the classical nature of Josephson phase and flux variables. In this context we also refer to the subjects of our presentation as "classical" analyses and modeling.

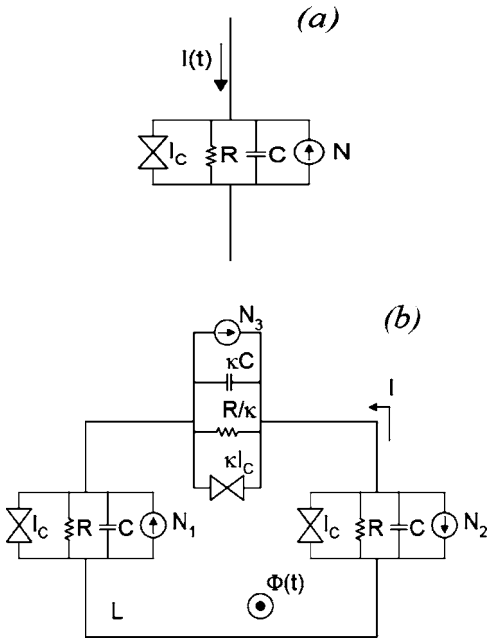

FIG. 1. Circuit diagram for (a) the single-junction model and (b) the three-junction loop. In (b) the smaller junction is indicated by the factor κ applied to the capacitance, resistance, and critical current.

II. THREE-JUNCTION LOOP RCSJ MODEL

A. Single-junction theory

Figure 1(a) depicts the single Josephson junction RCSJ model. Such a physical system is also referred to as single Josephson junction phase qubit. The normalized classical equation can be written as[24]

$$\ddot{\varphi} + \alpha\dot{\varphi} + \sin\varphi = \eta + \varepsilon_s \sin(\omega_s t + \theta_s) + \varepsilon_p(t) + n(t), \quad (1)$$

where φ is the difference between the phases of the quantum-mechanical wave functions defining the junction, η represents the dc bias current, and $\varepsilon_s(t)$ and ω_s represent microwave current amplitude and frequency, respectively. All currents are normalized to the critical current I_c, and time is measured in units of the inverse plasma frequency, ω_0^{-1}, where $\omega_0^2 = 2eI_c/\hbar C = 2\pi I_c/\Phi_0 C$, with C being the capacitance of the junction and $\Phi_0 = h/2e$ being the flux quantum. Tunneling of quasiparticles is represented by the dissipative term, where $\alpha = \hbar\omega_0/2eRI_c$ is given by the shunt resistance R, and the accompanying thermal fluctuations are time correlated by the normalized fluctuation-dissipation relationship,[36]

$$\langle n(t)\rangle = 0, \quad (2)$$

$$\langle n(t)n(t')\rangle = 2\alpha\frac{k_B T}{H_J}\delta(t-t') = 2\alpha\Theta\,\delta(t-t'), \quad (3)$$

with T being the temperature and H_J is the characteristic Josephson energy $H_J = I_c\hbar/2e$.

The normalized energy $(H - H_0)$ is defined by

$$H = \frac{1}{2}\dot{\varphi}^2 + 1 - \cos\varphi - \eta\varphi, \quad (4)$$

$$H_0 = 1 - \sqrt{1-\eta^2} - \eta\sin^{-1}\eta, \quad (5)$$

where H_0 is the energy at the minimum of a potential well. In Refs. 28 and 29 a classical analysis is presented for the modulated frequency, which is small when compared to the driving signal ω_s and referred to as the Rabi-type oscillation frequency Ω_R due to its direct relationship with experimentally reported Rabi oscillations. Thus, the classical analog to quantum-mechanical Rabi oscillations has been denoted as Rabi-type oscillations.[28]

B. Three-junction loop theory

Figure 1(b) depicts the three-junction loop which will be the subject of the analysis of this paper. We concentrate our study on this system which has been the core of several experiments and theoretical analyses.[35] It consists of a superconducting loop containing two identical junctions and one with smaller capacity and critical current. The normalized classical equations can be written as[35,37]

$$\ddot{\varphi}_1 + \alpha\dot{\varphi}_1 + \sin\varphi_1 = \frac{-1}{\beta_L}[2\pi M(t) + \varphi_1 + \varphi_2 + \varphi_3] + n_1(t),$$

$$\ddot{\varphi}_2 + \alpha\dot{\varphi}_2 + \sin\varphi_2 = \frac{-1}{\beta_L}[2\pi M(t) + \varphi_1 + \varphi_2 + \varphi_3] + n_2(t),$$

$$\ddot{\varphi}_3 + \alpha\dot{\varphi}_3 + \sin\varphi_3 = \frac{-1}{\kappa\beta_L}[2\pi M(t) + \varphi_1 + \varphi_2 + \varphi_3] + n_3(t), \quad (6)$$

where φ_i is the difference between the phases of the quantum-mechanical wave functions defining the ith junction, κ is the scale factor relating the one smaller junction, represented by φ_3, to the other two larger junctions, and β_L is the normalized loop inductance $\beta_L = 2\pi LI_c/\Phi_0$. $M(t)$ is a variable which sums up the external magnetic fluxes to which the system can be exposed;

$$M(t) = M_{\rm dc} + \varepsilon_s(t)\sin(\omega_s t + \theta_s) + \varepsilon_p(t), \quad (7)$$

where $M_{\rm dc}$ represents the flux of a time-independent field, $\varepsilon_s(t)$ and ω_s represent the ac flux (signal) amplitude and frequency, respectively, while a flux pulse for probing the state of the system is here taken into account by $\varepsilon_p(t)$. A general analysis of the above system of equations for arbitrary values of the parameters would surely lead to rather intriguing dynamics and complex oscillations. In the analysis that we will present herein we will focus on the limits that are suggested by the experimental reality. A very indicative example of the

effects that a finite inductance can have on Josephson flux qubit was reported in Ref. 34.

We write the Hamiltonian for the system as

$$H = H_k + H_p, \tag{8}$$

$$H_k = \frac{1}{2}(\dot{\varphi}_1^2 + \dot{\varphi}_2^2 + \kappa\dot{\varphi}_3^2), \tag{9}$$

$$H_p = 2 - \cos\varphi_1 - \cos\varphi_2 + \kappa(1 - \cos\varphi_3) + \frac{1}{2\beta_L}(\varphi_1 + \varphi_2 + \varphi_3 + 2\pi M)^2. \tag{10}$$

For small β_L in Eq. (8), we can see that energy from the loop current (last term) dominates the sum of the phases. We introduce now a transformation which allows combining the phases φ_1, φ_2, and φ_3 while maintaining the kinetic part of the Hamiltonian still separable in three distinct variables (ψ_1, ψ_2, and ψ_3);

$$\left.\begin{aligned}\psi_1 &= \varphi_1 + \varphi_2 + \varphi_3\\ \psi_2 &= \varphi_1 - \varphi_2\\ \psi_3 &= -\frac{1}{1+2\kappa}(\varphi_1 + \varphi_2) + \frac{2\kappa}{1+2\kappa}\varphi_3\end{aligned}\right\} \Leftrightarrow \begin{cases}\varphi_1 = \dfrac{\kappa}{1+2\kappa}\psi_1 + \dfrac{1}{2}\psi_2 - \dfrac{1}{2}\psi_3\\ \varphi_2 = \dfrac{\kappa}{1+2\kappa}\psi_1 - \dfrac{1}{2}\psi_2 - \dfrac{1}{2}\psi_3\\ \varphi_3 = \dfrac{1}{1+2\kappa}\psi_1 + \psi_3.\end{cases}$$

The Hamiltonian now becomes

$$H_k = \frac{1}{2}\left(\kappa\dot{\psi}_1^2 + \frac{1}{2}\dot{\psi}_2^2 + \frac{1}{2}(1+2\kappa)\dot{\psi}_3^2\right),$$

$$H_p = 2 - 2\cos\frac{\psi_2}{2}\cos\left(\frac{\kappa}{1+2\kappa}\psi_1 - \frac{1}{2}\psi_3\right) + \kappa\left[1 - \cos\left(\frac{1}{1+2\kappa}\psi_1 + \psi_3\right)\right] + \frac{1}{2\beta_L}(\psi_1 + 2\pi M)^2. \tag{11}$$

Under the condition $\beta_L \ll 1$, this system can be simplified to a single degree of freedom by examining the constraints which frame ψ_1 and ψ_2. First, it can be seen from Eq. (11) that potential energy considerations prevent the deviation of ψ_1 far from $-2\pi M$.

A second constraint, on ψ_2, is obtained by considering the equation of motion

$$\ddot{\psi}_2 + \alpha\dot{\psi}_2 + 2\cos\left(\frac{\kappa}{1+2\kappa}\psi_1 - \frac{1}{2}\psi_3\right)\sin\frac{\psi_2}{2} = n_1(t) - n_2(t).$$

From this it can seen that the static equilibrium value of ψ_2 is given by

$$\cos\frac{\psi_2}{2} = \begin{cases}1 & \text{for } \cos\left(\dfrac{\kappa}{1+2\kappa}\psi_1 - \dfrac{1}{2}\psi_3\right) > 0\\ -1 & \text{for } \cos\left(\dfrac{\kappa}{1+2\kappa}\psi_1 - \dfrac{1}{2}\psi_3\right) < 0.\end{cases} \tag{12}$$

Note that this is a *weak* constraint as it does not require much energy to break the equilibrium. Equation (11) can now be written as

$$H_p = 2 \mp 2\cos\left(\frac{\kappa}{1+2\kappa}\psi_1 - \frac{1}{2}\psi_3\right) + \kappa\left[1 - \cos\left(\frac{1}{1+2\kappa}\psi_1 + \psi_3\right)\right] + \frac{1}{2\beta_L}(\psi_1 + 2\pi M)^2, \tag{13}$$

where $\pm$ refers to the optimized choice based on Eq. (12). The constraint on ψ_1 can be determined by minimizing H_p with respect to ψ_1,

$$\frac{\partial H_p}{\partial\psi_1} = \frac{\pm 2\kappa}{1+2\kappa}\sin\left(\frac{\kappa}{1+2\kappa}\psi_1 - \frac{1}{2}\psi_3\right) + \frac{\kappa}{1+2\kappa}\sin\left(\frac{1}{1+2\kappa}\psi_1 + \psi_3\right) + \frac{1}{\beta_L}(\psi_1 + 2\pi M) = 0$$

$$\Rightarrow \psi_1 = -2\pi M - \beta_L\delta_1 \approx -2\pi M - \beta_L\frac{\kappa}{1+2\kappa} \times\left[\mp 2\sin\left(\frac{2\pi M\kappa}{1+2\kappa} + \frac{1}{2}\psi_3\right) + \sin\left(\psi_3 - \frac{2\pi M}{1+2\kappa}\right)\right],$$

which is correct to first order in β_L.

The potential energy can now be approximated by a function of ψ_3 only,

$$H_p = 2 \mp 2\cos\left(\frac{2\pi M\kappa}{1+2\kappa} + \frac{1}{2}\psi_3\right) + \kappa - \kappa\cos\left(\psi_3 - \frac{2\pi M}{1+2\kappa}\right) - \frac{\beta_L}{2}\delta_1^2,$$

where the choice between $\mp$ should be such that the energy is minimized.

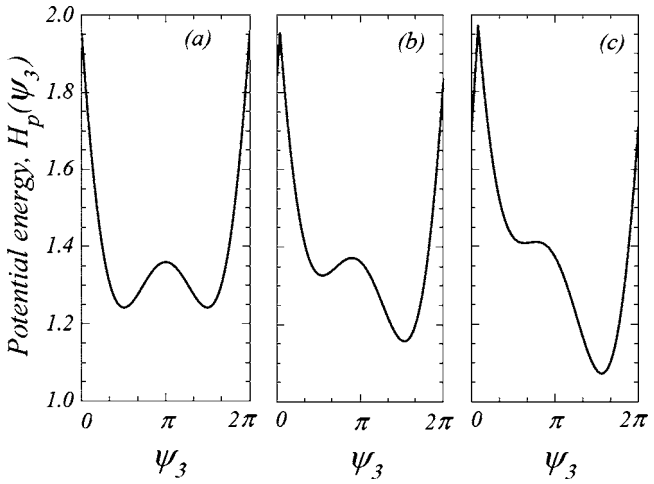

FIG. 2. Three-junction loop potential Energy in terms of the reduced variable ψ_3. Each view represents a different value of M_{dc}: (a) $M_{dc}=0.5$, (b) $M_{dc}=0.52$, and (c) $M_{dc}=0.542$. Other parameters are $\kappa=0.68$ and $\beta=0.09559$.

Figure 2 depicts this single-degree-of-freedom representation of the potential energy. Note that while, in general, this potential consists of pairs of wells separated by higher energy "cusps," for purposes of this work we focus on a single pair of wells as the energies are kept below these cusps.

Calculating the linear resonance frequency for a given well, the equation of motion for the frictionless and constant-M system is

$$\frac{1}{2}(1+2\kappa)\ddot{\psi}_3+\frac{\partial H_p}{\partial \psi_3}=0$$

such that the fixed point ψ_3^* is given by

$$\left.\frac{\partial H_p}{\partial \psi_3}\right|_{\psi_3=\psi_3^*}=0$$

and for small oscillations δ around the fixed point $\psi_3=\psi_3^*+\delta$ provides the linear resonance frequency ω_l,

$$\frac{1}{2}(1+2\kappa)\ddot{\delta}+\left.\frac{\partial^2 H_p}{\partial \psi_3^2}\right|_{\psi_3^*}\delta=0\Rightarrow \tag{14}$$

$$\omega_l=\sqrt{2\left.\frac{\partial^2 H_p}{\partial \psi_3^2}\right|_{\psi_3^*}}(1+2\kappa). \tag{15}$$

In Sec. III we will use this result to characterize the switching statistics of microwave induced excitations in the classical model of the three-junction superconducting loop.

III. SIMULATION RESULTS

Our system is periodic under the application of the external magnetic flux. In order to best describe the experimental reality the temperatures that we consider are in the tens of millikelvin range: we point out, however, that the kind of phenomena such as those that we shall describe herein have been characterized in a temperature range spanning from few tens of mK up to 800 mK (Ref. 32); we believe that most of the phenomena herein described would display quite similar dependencies on temperature over the same range.

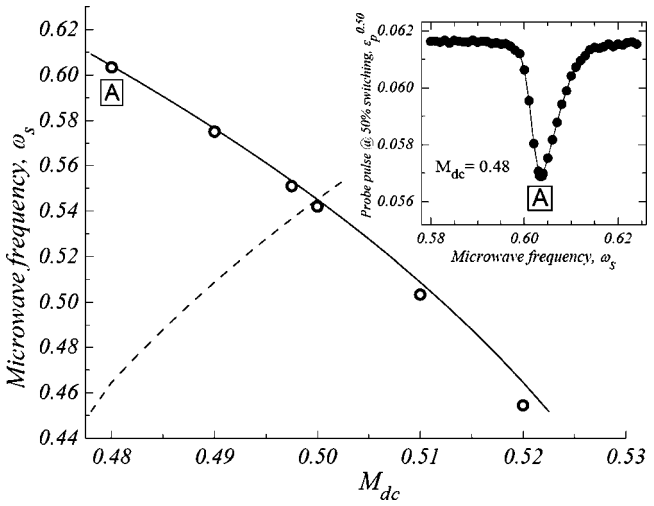

FIG. 3. Resonant frequency response in the three-junction loop. Lines represent the predicted frequency response from Eq. (14). The open circles indicate the resonances from the results of our simulations. The inset is a switching distribution indicating the resonance at the box marked "A." This provides an example of the placement for the open circles in the larger plot. Parameters for the simulation were $\beta_L=0.09994$, $\kappa=0.68$, $\alpha=4\times10^{-5}$, $\varepsilon_s=4\times10^{-4}$, and $\Theta(T)=9.12\times10^{-3}$. The dashed line indicates the symmetric relationship in linear resonance frequency. The data presented are based on 2500–7000 escape events.

To verify Eq. (14), we conducted computer simulations of pulsed microwave spectroscopy for the three-junction loop described by Eqs. (6); naturally, the simulations are performed on the entire system of equations regardless of the analytical approximations. Microwave spectroscopy, combined with thermal escape measurements, has turned out to be a reliable tool for investing resonances.[25–27] Here we try to follow real experimental recipes;[33] we must bear in mind that for the thermal escape we simulate the whole system of Eqs. (6) and that switching events to voltage states are just detected across a parallel connection of two junctions which forces us to attribute a 50% equal probability of switching to the two junctions. The results of our tracing the resonance through thermal escape and microwave pulses are shown in Fig. 3. Each open circle represents the minimum flux pulse ε_p required to obtain a statistical response of 50% escape probability. Each trial in the simulation is conducted in the following manner: with initial conditions of ψ_3 in the minimum energy configuration and $\dot{\psi}_3=0$, the system is driven at frequency ω_s and amplitude ε_s for a period of $(2/\alpha)$. At the end of the driving phase and after a slight pause (50 time units), a pulse of magnitude ε_p is applied (in similar fashion to Ref. 30) and the subsequent escape or non-escape to the alternate well is recorded. Statistics are then gathered to determine $\varepsilon_p^{50\%}$ for varying frequency. A resonance is determined for each value of M_{dc}, as indicated by a minimum value of $\varepsilon_p^{50\%}$ as a function of frequency. In the inset of Fig. 3 we show the resonance effect in terms of switching probability, exemplified for the point labeled by the A box (close to the vertical axis in the figure).

The solid line in Fig. 3 represents the resonant frequency response as predicted by Eq. (14). The open circles indicate the simulation results and depict the minimum amplitude probe pulse ε_p for which the escape rate equals 50%. The inset shows the relationship between probe pulse (at 50% escape probability) and signal frequency for $M_{\mathrm{dc}}=0.48$. The minimum energy value in each well is marked with a boxed symbol to establish the correspondence with the potential energy plot. The dashed line indicates the symmetric relationship in linear resonance frequency (about $M_{\mathrm{dc}}=0.5$) for a well placement convention which is opposite to that of the continuous curve: in other terms, in the continuous line, we trace the resonance moving the lower energy well (follow Fig. 2) from left to right while the dashed line would correspond to tracing the resonance moving the lower energy well from right to left. The data presented are based on 2500–7000 escape events; the simulation results show close agreement with our theory although the agreement diminishes slightly for increasing values of M_{dc}. This can be understood by noting that as the flux bias is increased, the higher of the two wells becomes broader, allowing larger oscillations, which corresponds to a greater degree of anharmonic behavior.

Next we investigated whether the results obtained on the linear resonance frequency calculated from Eq. (14) will generate features consistent with what one could expect from spectroscopic measurements on real Josephson junction systems. Thus we tuned the parameters of our simulations to generate Rabi-type oscillations, Ramsey-type fringes, and spin-echo-type oscillations.[30–32] The recipes for generating these oscillations follow closely the ones described in the previous publications for the single-junction model; and a summary of the signaling used for generating Rabi-type oscillations, Ramsey-type fringes, and spin echo is shown in Fig. 4 together with the idealized phase responses in the two relevant cases of escape and no escape from the potential well. Our statistical simulation results are shown in Figs. 5 and 6. The normalized slope that we extract from the linear dependency of the Rabi frequency versus ac amplitude of Fig. 5(b) is very close to that of the experimental results reported in Fig. 4(b) of Ref. 12 and with Fig. 4(b) of Ref. 10. We conclude that our numerical and analytical results are quite consistent with the experimental reality. As far as the Ramsey-type fringes are concerned, if we compare Fig. 5(d) in this presentation with the results reported in Fig. 4(d) of Ref. 12, we also find very good agreement in the Ramsey-type fringe being represented by a unity-sloped V-shaped fringe frequency dependence on the microwave detuning from the oscillator resonance. We clearly see our V shape following the dashed lines in Fig. 5(d). Thus, just as it has been demonstrated for Rabi oscillations, the classical system exhibits a signature similar, if not identical, to what one would expect from quantum theory.

We note that our analytical approximations explain how the three-loop potential can be reduced to a single-degree-of-freedom potential. However, it is clear from the results of the direct integration of Eqs. (6) shown in Fig. 6 that the response of the loop is quite similar to that of a single junction.[30,31]

The classical result, leading to the Ramsey-fringe frequency being identical to the detuning between the applied microwave frequency ω_s and the intrinsic resonance ω_r of the oscillator, can be rationalized by considering the system behavior in the interval between the two $\pi/2$ pulses. The

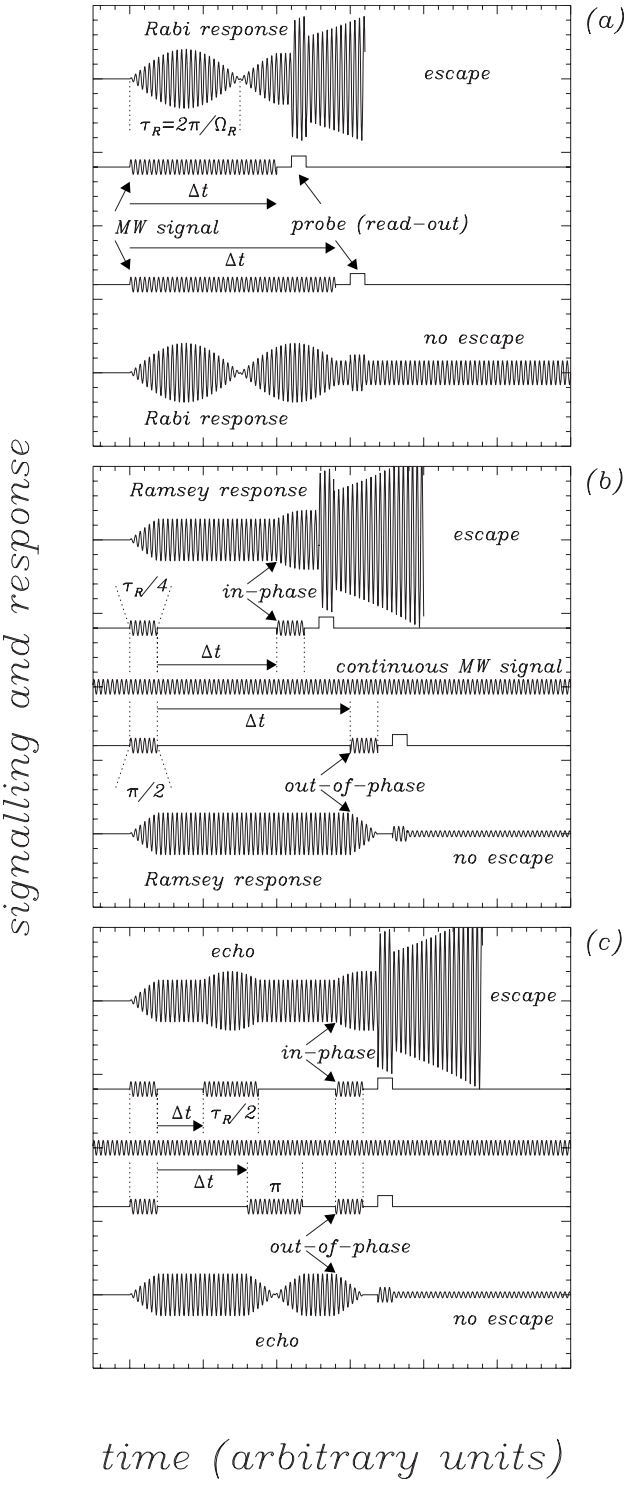

FIG. 4. Sketches of idealized microwave perturbations and corresponding classical system (phase) responses for (a) Rabi oscillations, (b) Ramsey fringes, and (c) spin echo. Upper part of each plot illustrates a situation in which the probe (read-out) pulse results in an escape from the potential well, while the lower part illustrates a no-escape case. The experimentally varied time for observing the oscillations in response is shown on each plot as Δt.

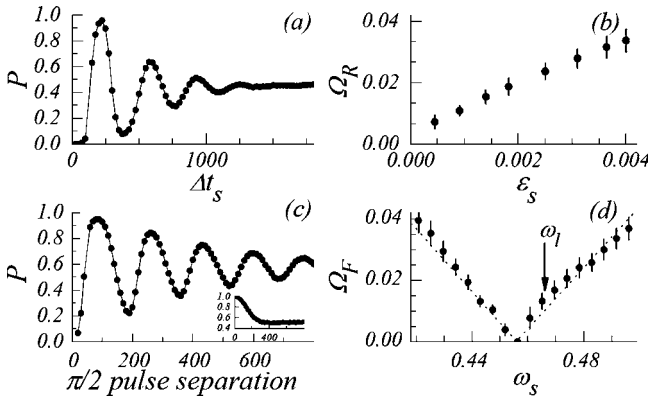

FIG. 5. Oscillation phenomena for the three-junction loop: Rabi-type oscillations and Ramsey-type fringes. Panel (a) shows Rabi-type oscillations. Panel (b) indicates the Rabi-type frequency as a function of microwave amplitude, with ε_s for $\omega_s=0.45629\sim\omega_r$. Panel (c) is the resulting switching distribution for Ramsey-type fringes with $\omega_s=0.42528$ and $\varepsilon_p=0.0195$. The inset depicts the driving frequency which achieves a fringe frequency of zero; here $\omega_s=0.45629\sim\omega_r$ and $\varepsilon_p=0.0148$. Panel (d) provides the relationship between fringe frequency and driving frequency. The arrow indicates measurement of $\omega_l=0.46557$ by direct simulation. Note that Eq. (14) predicts $\omega_l=0.46625$. Parameters for all panels, unless otherwise noted, were $M_{\rm dc}=0.52$, $\beta_L=0.09559$, $\kappa=0.68$, $\alpha=1.5\times10^{-4}$, $\varepsilon_s=1.82\times10^{-3}$, $\omega_s=0.443$, $\varepsilon_p=0.0149$, and $\Theta(T)=3\times10^{-3}$; statistics were gathered for ~20 000 escape events.

oscillator is, at the time of the conclusion of the first $\pi/2$ pulse, defined by a specific phase relationship (phase locking) to the phase of the pulse. This phase relationship is free to detune in the (ballistic) interval Δt between the two $\pi/2$ pulses, and the mutual phase detuning θ_F between the microwave field and the oscillator is therefore given by

$$\theta_F=\int_0^{\Delta t}[\omega_s-\omega_r(t)]dt,$$

where ω_r can be a (weak) function of time due to the anharmonicity of the potential energy; i.e., as the oscillation amplitude decreases, due to the intrinsic damping in the system, the natural resonance frequency of the oscillator increases.

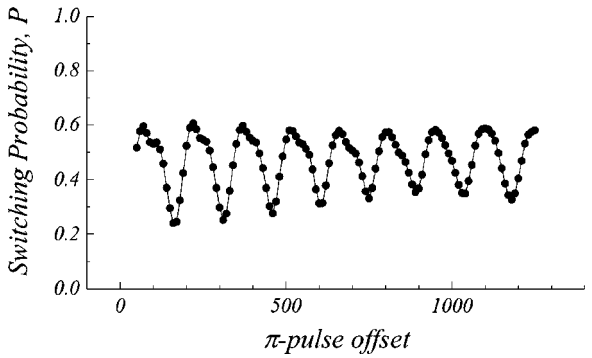

FIG. 6. Spin-echo-type oscillations for three-junction loop. Parameters are $M_{\rm dc}=0.52$, $\beta_L=0.09559$, $\kappa=0.68$, $\alpha=1.5\times10^{-4}$, $\omega_s=0.419787$, $\varepsilon_s=1.82\times10^{-3}$, $\varepsilon_p=0.0195$, and $\Theta(T)=3\times10^{-3}$. Each dot represents 22 000 escape events.

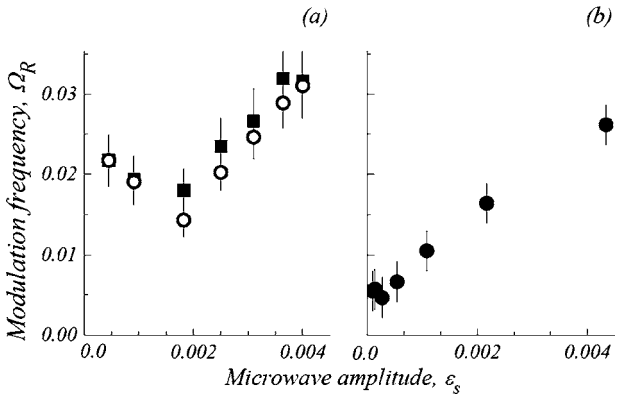

FIG. 7. Simulations of off-resonance Rabi-type oscillation frequencies. Panel (a) depicts the off-resonance modes for the three-junction loop. Parameters were: $M_{\rm dc}=0.52$, $\beta_L=0.09559$, $\kappa=0.68$, $\omega_s=0.443$, $\varepsilon_s=1.82\times10^{-3}$, $\varepsilon_p=0.063$, and $\Theta=3\times10^{-3}$. Two values of characteristic damping are given. The filled squares correspond to $\alpha=1.5\times10^{-4}$; empty circles: $\alpha=0$. The resonance frequency ω_r [as shown in Fig. 5(d)] is 0.45629. Panel (b) shows the off-resonance modes for the single-junction circuit. Parameters were $\alpha\sim1.5\times10^{-4}$, $\eta=\sqrt{1-\omega_l^4}$, $\omega_s=0.99$, $\omega_l=0.646188$, and $\Theta=2\times10^{-4}$.

However, for a lightly damped system, where $\alpha\Delta t\ll1$, the above time integration can be simplified, and the result for the Ramsey-fringe frequency Ω_F becomes

$$\Omega_F=\frac{\theta_F}{\Delta t}\approx\omega_s-\omega_r,$$

which is exactly the detuning between the applied microwave frequency and the natural resonance frequency of the oscillator in the phase-locked state. Thus, the observed Ramsey-fringe frequency dependence on the microwave detuning from resonance is easily understood classically for this system, and the intrinsic oscillator frequency $\omega_r\lesssim\omega_l$ is close to the microwave frequency that results in $\Omega_F\approx0$. We submit that this detuning is also causing the so-called spin-echo measurements, which are generated by maintaining a constant temporal separation between the two $\pi/2$ pulses from Ramsey-fringe measurements and then inserting a π pulse. The final phase relationship between the oscillator and the external microwave signal is detected by the second $\pi/2$ pulse, but this phase relationship is now subject to the phase twisting caused by the inserted π pulse, which in turn depends on the detuning at the time of π-pulse initiation. Thus, while the Rabi frequency determines the magnitude and duration of the microwave pulses used in Ramsey-fringe experiments, it is the Ramsey-fringe frequency that determines the echo from the detuning at the time of the initiation of the π pulse.[31]

In previous work, and here in Fig. 5(b), we have considered Rabi-type oscillations using the resonant frequency as the driving frequency: $\omega_s=\omega_l\cong\omega_r$. However, this is not necessarily the case for all experiments. In Fig. 7 we show the effect of a lower-than-resonance ($\omega_s<\omega_l$) driving signal on Rabi-type frequency. One important aspect of these plots is that low-amplitude signals result in modulation frequencies

which do not lie on the "main sequence" curve to which higher-amplitude responses conform. We assert that the reason for this is found in the multivalued nature of the amplitude (and energy) response for off-resonant driving as shown in Ref. 27, Fig. 1. Also notable is the fact that this effect (an analytical result for the single junction) is also seen in the three-junction loop.

IV. CONCLUSIONS

The analysis we have developed reducing the three-junction loop to a single degree of freedom provides a significant reduction in the complexity of the system. The resulting equation provides direct agreement with our simulations when identifying the system resonances from experimentally relevant switching experiments.

Our studies of off-resonant driving of Rabi-type oscillations reinforce earlier work concerning multivalued functions in signal amplitude. Although no distinct conclusions can be made with regard to a connection between off-resonant driving signals and linear relationships between Rabi-type frequency and signal amplitude, we have shown evidence that driving the system near (but not exactly at) resonance does extract nearly linear behavior in the response for larger amplitudes. We emphasize that the simple model we are using may not completely account for all the details of the observed phenomena.

Consistently with our previous work, we have used the classical RCSJ phenomenology to investigate various phenomena heretofore attributed to macroscopic quantum tunneling and we have shown very good agreement with experimental results so far reported. We have shown that, with regard to Rabi-type oscillations, Ramsey-type fringes, and spin-echo-type oscillations, the three-junction loop differs little, qualitatively, from the single-junction circuit. This is easily attributed to the fact that the important dynamics of these systems is governed by resonant excitations in anharmonic potential wells followed by a read-out perturbation which makes it possible for the system to escape from the well. Thus, our developed analysis and intuition about the system response to applied microwave pulses translate easily from a simple single-junction system to other systems with similar overall resonant excitations and escape from anharmonic wells. The main difference between the single-junction system and other systems, such as the three-loop system studied here, is that the experimental reality may be different. However, given the relative insensitivity to noise inherent in the three-junction loop, it is understandable that several research groups work with flux qubits rather than single junctions (biased by dc bias current supplies).

The work herein presented was developed on the background of the Ph.D. thesis[32] of one of the authors (J.E.M.) which was submitted to the University of California at Davis in the fall of 2006. In the present paper we have chosen to keep the same terminology (Rabi-type oscillations, Ramsey-type fringes, etc.) introduced in the thesis and in the papers which inspired it.[25–28] Other authors have recently reported on RCSJ-based analysis of the three-junction Josephson system presenting their own terms and analysis.[38] In these papers, the pumping by an ac drive was used in order to generate low frequency modulations of phase and energy, and the conclusions confirm a nonlinear phenomenon reported previously in simulations and experiments;[25–27,39] namely, that it is possible to phase-lock Josephson systems by superharmonic pumping. The quantum effects on the other hand should not be sensitive to the superharmonic drive and therefore this difference could constitute a discriminant between classical and quantum effects. Two of us (M.C. and N.G.J.) were co-authors in publications[25,26] in which the superharmonic pumping of phase qubit was observed over a broad temperature range: we recall indeed that nonlinear RCSJ dynamics can model a Josephson system over broad parameter ranges and in particular at very low temperatures. Recent observations[34] indicate that this is indeed the case down to 10 mK where striking experimental observations of nonlinear effects are observed; therefore, it might not be easy to engineer a Josephson system on which all the nonlinear effects are purged out. It is also worth noticing that it is not straightforward to draw conclusions from experiments with superharmonic pumping of a superconducting circuit due to the varying responses that both the system and the microwave apparatus may have at different frequencies.

The possibility that the behavior of a physical system thought to demonstrate evidence of macroscopic quantum superposition can be interpreted with a different approach is not a unique characteristic the Josephson effect. Roughly three decades ago scientists were looking for macroscopic quantum effects in charge density-wave systems,[40] and it was found that the reported results could also be explained by alternative and more "classical" models.[41] It was earlier speculated that these kind of arguments would not find space and motivation in Josephson systems, but while our findings for resonant switching, Rabi oscillations, Ramsey fringes, and spin echo do not preclude observations of quantum behavior in Josephson systems, the evidence of recent years has shown that many observed phenomena in this class of systems can be attributed to the RCSJ dynamics developed for Josephson variables in a classical limit.[24]

ACKNOWLEDGMENTS

We wish to thank John Clarke, Alexey Ustinov, Paul Reichardt, and Travis Hime for taking the time to assist us in this endeavor. This work was supported in part by the UC Davis Center for Digital Security under the USA AFOSR (Grant No. FA9550-04-1-0171).

[1] *Quantum Computing and Quantum Bits in Mesoscopic Systems*, edited by A. Leggett, B. Ruggiero, and P. Silvestrini (Kluwer Academic/Plenum, New York, 2004).
[2] P. Silvestrini, V. Palmieri, B. Ruggiero, and M. Russo, Phys. Rev. Lett. **79**, 3046 (1997); P. Silvestrini, B. Ruggiero, C. Granata, and E. Esposito, Phys. Lett. A **267**, 45 (2000).
[3] J. M. Martinis, S. Nam, J. Aumentado, and C. Urbina, Phys. Rev. Lett. **89**, 117901 (2002).
[4] R. W. Simmonds, K. M. Lang, D. A. Hite, S. Nam, D. P. Pappas, and J. M. Martinis, Phys. Rev. Lett. **93**, 077003 (2004).
[5] A. Wallraff, T. Duty, A. Lukashenko, and A. V. Ustinov, Phys. Rev. Lett. **90**, 037003 (2003).
[6] J. Claudon, F. Balestro, F. W. J. Hekking, and O. Buisson, Phys. Rev. Lett. **93**, 187003 (2004).
[7] A. Wallraff, D. I. Schuster, A. Blais, L. Frunzio, J. Majer, M. H. Devoret, S. M. Girvin, and R. J. Schoelkopf, Phys. Rev. Lett. **95**, 060501 (2005).
[8] C. H. van der Wal, A. C. J. ter Haar, F. K. Wilhelm, R. N. Schouten, C. J. P. M. Harmans, T. P. O. S. Lloyd, and J. E. Mooij, Science **290**, 773 (2000).
[9] I. Chiorescu, Y. Nakamura, C. J. P. M. Harmans, and J. E. Mooij, Science **299**, 1869 (2003).
[10] E. Il'ichev, N. Oukhanski, A. Izmalkov, Th. Wagner, M. Grajcar, H.-G. Meyer, A. Yu. Smirnov, A. Maassen van den Brink, M. H. S. Amin, and A. M. Zagoskin, Phys. Rev. Lett. **91**, 097906 (2003).
[11] T. Kutsuzawa, H. Tanaka, S. Saito, H. Nakano, K. Semba, and H. Takayanagi, Appl. Phys. Lett. **87**, 073501 (2005).
[12] B. L. T. Plourde, T. L. Robertson, P. A. Reichardt, T. Hime, S. Linzen, C. E. Wu, and J. Clarke, Phys. Rev. B **72**, 060506(R) (2005).
[13] S. Saito, T. Meno, M. Ueda, H. Tanaka, K. Semba, and H. Takayanagi, Phys. Rev. Lett. **96**, 107001 (2006).
[14] D. Vion, A. Aasime, A. Cottet, P. Joyez, H. Pothier, C. Urbina, D. Esteve, and M. H. Devoret, Science **296**, 886 (2002).
[15] J. R. Friedman, V. Patel, W. Chen, S. K. Tolpygo, and J. E. Lukens, Nature (London) **406**, 43 (2000).
[16] Y. Nakamura, Y. A. Pashkin, and J. S. Tsai, Phys. Rev. Lett. **87**, 246601 (2001).
[17] Y. A. Pashkin, T. Yamamoto, O. Astafiev, Y. Nakamura, D. V. Averin, and J. S. Tsai, Nature (London) **421**, 823 (2003).
[18] R. H. Koch, J. R. Rozen, G. A. Keefe, F. M. Milliken, C. C. Tsuei, J. R. Kirtley, and D. P. DiVincenzo, Phys. Rev. B **72**, 092512 (2005).
[19] P. Bertet, I. Chiorescu, G. Burkard, K. Semba, C. J. P. M. Harmans, D. P. DiVincenzo, and J. E. Mooij, Phys. Rev. Lett. **95**, 257002 (2005).
[20] I. I. Rabi, Phys. Rev. **51**, 652 (1937).
[21] N. F. Ramsey, Phys. Rev. **78**, 695 (1950).
[22] D. Vion, A. Aasime, A. Cottet, P. Joyez, H. Pothier, C. Urbina, D. Esteve, and M. H. Devoret, Fortschr. Phys. **51**, 462 (2003).
[23] M. Steffen, M. Ansmann, R. C. Bialczak, N. Katz, E. Lucero, R. McDermott, M. Neeley, E. M. Weig, A. N. Cleland, and J. M. Martinis, Science **313**, 1423 (2006).
[24] T. Van Duzer and C. W. Turner, *Principles of Superconducting Devices and Circuits* (Elsevier, New York, 1998); A. Barone and G. Paternò, in *Physics and Applications of the Josephson Effect* (Wiley and Sons, New York, 1982); For the derivation of the classical nature of Josephson variables and related analogy with pendulum Hamiltonians, see P. W. Anderson, in *Lectures on the Many Body Problem*, edited by E. R. Caianiello (Academic, New York, 1964), Vol. 2, p. 132.
[25] N. Grønbech-Jensen, M. G. Castellano, F. Chiarello, M. Cirillo, C. Cosmelli, L. V. Filippenko, R. Russo, and G. Torrioli, Phys. Rev. Lett. **93**, 107002 (2004).
[26] N. Grønbech-Jensen, M. G. Castellano, F. Chiarello, M. Cirillo, C. Cosmelli, V. Merlo, R. Russo, and G. Torrioli, in *Quantum Computing: Solid State Systems*, edited by B. Ruggiero, P. Delsing, C. Granata, Y. Paskin, and P. Silvestrini (Kluwer Academic and Springer, New York, 2005), pp. 111–119; this paper also appeared in arXiv:cond-mat/0412692.
[27] N. Grønbech-Jensen and M. Cirillo, Phys. Rev. B **70**, 214507 (2004).
[28] N. Grønbech-Jensen and M. Cirillo, Phys. Rev. Lett. **95**, 067001 (2005).
[29] J. E. Marchese, M. Cirillo, and N. Grønbech-Jensen, Phys. Rev. B **73**, 174507 (2006).
[30] J. E. Marchese, M. Cirillo, and N. Grønbech-Jensen, Open Syst. Inf. Dyn. **14**, 189 (2007).
[31] J. E. Marchese, M. Cirillo, and N. Grønbech-Jensen, Eur. Phys. J. Spec Top. **147**, 333 (2007).
[32] J. E. Marchese, Ph.D. thesis, University of California, Davis, 2007. Part of the results of this thesis, including the ones concerning the three-junction loop system, were presented by one of us (N.G.J.) at the "International Workshop on Solid-State Quantum Computing" (Nanjing, China, 9–12 June 2006).
[33] M. Cirillo, P. Carelli, M. G. Castellano, F. Chiarello, C. Cosmelli, N. Grønbech-Jensen, R. Leoni, J. E. Marchese, F. Mattioli, D. Simeone, and G. Torrioli, Physica C **437-438**, 46 (2006).
[34] M. G. Castellano, F. Chiarello, R. Leoni, F. Mattioli, G. Torrioli, P. Carelli, M. Cirillo, C. Cosmelli, A. de Waard, G. Frossati, N. Grønbech-Jensen, and S. Poletto, Phys. Rev. Lett. **98**, 177002 (2007).
[35] T. P. Orlando, J. E. Mooij, L. Tian, C. H. van der Wal, L. S. Levitov, S. Lloyd, and J. J. Mazo, Phys. Rev. B **60**, 15398 (1999).
[36] G. Parisi, *Statistical Field Theory* (Addison-Wesley, Reading, MA, 1988).
[37] U. Geigenmüller, J. Appl. Phys. **80**, 3934 (1996).
[38] A. N. Omelyanchouk, S. N. Shevchenko, A. M. Zagoskin, E. Il'ichev, and F. Nori, Phys. Rev. B **78**, 054512 (2008); S. N. Shevchenko, A. N. Omelyanchouk, A. M. Zagoskin, S. Savel'ev, and F. Nori, New J. Phys. **10**, 073026 (2008).
[39] M. Cirillo, G. Rotoli, A. R. Bishop, N. Grønbech-Jensen, and P. S. Lomdahl, Phys. Rev. B **52**, 506 (1995); M. Cirillo, V. Merlo, D. Winkler, and N. Thyssen, IEEE Trans. Appl. Supercond. **9**, 3745 (1999).
[40] J. Bardeen, Phys. Rev. Lett. **42**, 1498 (1979); R. E. Thorne, J. R. Tucker, and J. Bardeen, *ibid.* **58**, 828 (1987).
[41] L. Sneddon, M. C. Cross, and D. S. Fisher, Phys. Rev. Lett. **49**, 292 (1982); R. A. Klemm and J. R. Schrieffer, *ibid.* **51**, 47 (1983).